Enhancing the deformation range of ionic polymer metal composites through electrostatic actuation

A. Boldini,[1,a)] K. Jose,[1,a)] Y. Cha,[2] and M. Porfiri[1,b)]
[1]*Department of Mechanical and Aerospace Engineering, Tandon School of Engineering, New York University, Brooklyn, New York 11201, USA*
[2]*Center for Intelligent & Interactive Robotics, Korea Institute of Science and Technology, Seoul 02792, South Korea*

(Received 28 April 2018; accepted 11 June 2018; published online 27 June 2018)

The large range of deformations of ionic polymer metal composites (IPMCs) has often been proposed as a key advantage of these soft active materials. Nevertheless, many applications in soft robotics still cannot be addressed by current IPMC technology, demanding an even wider deformation range. Here, we empirically demonstrate the feasibility of integrating electrostatic actuation to enhance IPMC deformations. Through the use of external contactless electrodes, an electrostatic pressure is generated on the IPMC, thereby magnifying the deformation elicited by the small voltage applied across its electrodes. A mathematical model is established to predict the onset of the pull-in instability, which defines when electrostatic actuation can be effectively utilized to enhance IPMC performance. *Published by AIP Publishing*. https://doi.org/10.1063/1.5037889

Ionic polymer metal composites[1,2] (IPMCs) are a class of soft active materials with a wide range of engineering and medical applications, including underwater propulsion systems,[3] catheter platforms,[4] microgrippers,[5] and intra-ocular lens systems.[6] With recent advancements in three-dimensional printing,[7] applications are quickly growing, opening the door to a pervasive use of IPMCs, beyond the reach of other soft materials. In its basic incarnation, an IPMC is a sandwich composite made from an ionomeric core (usually Nafion^{TM}) saturated with mobile counterions. Noble metal layers are plated on each side of the ionomer to serve as electrodes. Upon applying a voltage across the electrodes, redistribution of mobile counterions leads to a number of concurrent chemoelectromechanical phenomena,[8–11] triggering its macroscopic deformation.

While their large deformation range has often been proposed as a key advantage,[12,13] several scientific and engineering applications call for even larger deformations. For example, IPMCs have been successfully utilized as underwater propulsion systems in biologically inspired robotic fish,[3] but their current deformation range limits the cruise speeds of the prototypes and challenges the implementation of C- and U-turns that are common to swimming fish.[14] The IPMC deformation range is practically constrained by the moderate voltage signals that can be applied without damaging the ionomer and the electrodes. For voltages higher than 6 V, dielectric breakdown of the solvent may, in fact, occur.[15,16] In order to overcome this limitation, various techniques have been reported in the literature.[17] They predominantly involve modification of the electrode surface (plasma treatment,[18] introduction of nanostructures,[19] or coating with parylene[20]) or modification of the ionomer (through foaming,[21] thickness manipulation,[22] or polypyrrole/alumina filler incorporation[23]).

In this letter, we propose an alternative approach for enhancing IPMC deformation. Rather than attempting at a targeted modification of its microstructure, we propose an authentic multiphysics solution that capitalizes on the inherent multifunctionality of IPMCs. Specifically, we put forward the integration of auxiliary electrostatic forces acting on the IPMC electrodes to enhance internal actuation. Similar to a comb-drive actuator,[24] we place an IPMC between two external electrodes at the same voltage V_{Wall} with respect to a common ground, see Fig. 1(a). These external electrodes create an electric field which interacts with the surface charges on the IPMC electrodes to generate an electrostatic pressure on the IPMC. If the IPMC electrodes are short-circuited to the common ground, the electrostatic pressure on the two IPMC electrodes should be balanced and the IPMC will maintain its vertical position. On the other hand, if a small voltage, V_{IPMC}, is applied across the IPMC electrodes, the electrostatic pressure will not be balanced and the IPMC will experience a magnified deformation.

While electrostatic actuation of IPMCs is untapped, contactless actuation of plain Nafion^{TM} has recently been demonstrated by Kim *et al.*[25] Through an oscillating external electric field, Nafion^{TM} microfibers were activated in an electrolyte solution. Similar to cilia microorganisms, the microactuators exhibited a cyclic response, due to a net counterion current through the ionomer. This actuation mechanism is radically different from the Coulomb forces, which require charge storage at the IPMC electrodes rather than immersion in an electrolyte solution.

As discovered by Nathanson and colleagues half a century ago,[26] electrostatic actuation is confined to a given voltage window, whereby voltage levels exceeding a critical value will cause the actuator to quickly approach one of the external electrodes and potentially stick to it. This phenomenon is known as pull-in instability and its precise quantification as a function of the physical and geometric properties of the actuator is the object of intense research in microelectromechanical systems.[27–29] The basic mechanism underlying pull-in is the softening effect induced by the nonlinear

[a)]A. Boldini and K. Jose contributed equally to this work.
[b)]Author to whom correspondence should be addressed: mporfiri@nyu.edu

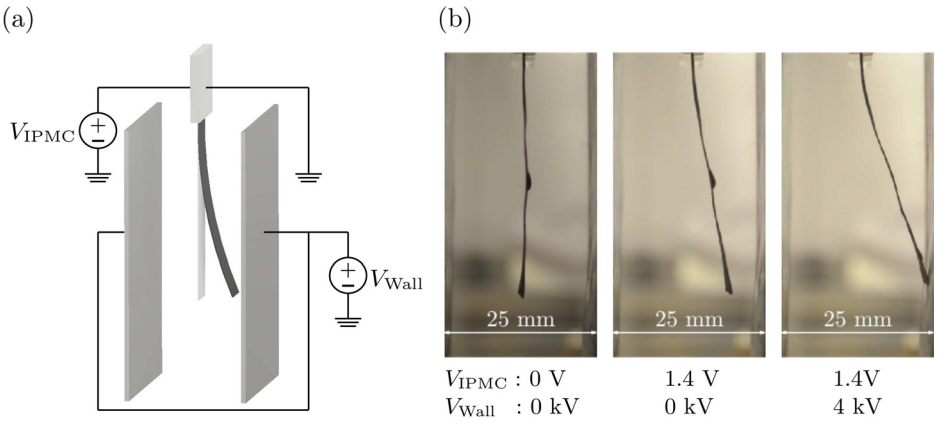

FIG. 1. (a) Schematics of the experimental setup. The lighter shape indicates the undeformed configuration of the IPMC, while the darker shape represents its deformed configuration. (b) IPMC deflection for different experimental conditions. From left to right: initial shape without actuation; deflection due to internal actuation; and deflection induced by simultaneous internal and electrostatic actuation.

electrostatic pressure, which counters the restoring role of the mechanical stiffness. As a result of pull-in, the integration of electrostatic actuation within the design of IPMC actuators should be feasible only for a range of actuation voltages. The experimental identification of this operating range and its theoretical prediction are the chief aims of this letter.

To demonstrate our approach, we conduct experiments on an IPMC of length 45 mm, width 9 mm, and thickness 0.27 mm (the sample was fabricated by the Active Materials and Smart Living Laboratory at the University of Nevada Las Vegas). The IPMC is installed in clamps on which copper conductive strips are attached, such that a voltage can be applied to the sample during the tests. The clamps are attached to a supporting structure that allows the positioning of the sample between two external copper electrodes. This structure can be shifted along the vertical direction to facilitate the installation of the IPMC. The IPMC is positioned at a free length of 40 mm and a nominal gap of $g_0 = 12.5$ mm from each of the external electrodes. We acknowledge that the tip could be closer to one of the external electrodes at the beginning of the test, due to some eccentricity of the specimen. External electrodes are covered with a 0.06 mm thick anti-static plastic sheet to prevent direct contact with the IPMC and avoid unwanted residual charges after application of high voltage to the external electrodes.

A driving circuit, capable of imposing a voltage V_{IPMC} up to 2 V on the IPMC and a voltage V_{Wall} up to 4 kV across the external electrodes, is designed and built in-house. A microcontroller (Arduino Uno) is interfaced with a dual channel digital-to-analog converter (DAC, MCP4822). The two output channels of the DAC are fed into the two non-inverting terminals of a dual channel op-amp (L272A) in unity gain buffer configuration on both channels. One of the output channels of the op-amp is connected to the IPMC via a 2P3T toggle switch, which allows for the inversion of V_{IPMC} polarity. The other op-amp output channel is connected to the input of a high voltage DC-DC converter, whose output (at V_{Wall}) is connected to the external electrodes. The microcontroller, via serial communication, is interfaced with a laptop whose custom software allows for controlling the actuation voltage pair (V_{IPMC}, V_{Wall}). Five experiments have been recorded with a Nikon D90 DSLR camera for image post-processing, conducted with an in-house developed code on Matlab® at a resolution of 60 μm.

Figure 1(b) shows three frames from the recordings of the trials. The frame on the left displays the initial shape of the IPMC before the application of the actuation voltages. The initial eccentricity of the IPMC may be present due to uneven water hydration of the sample, emphasized by the electroless plating process for the metal electrodes.[30] In the middle frame, the deflection of the IPMC following the application of a small voltage V_{IPMC} is shown. In this case, the external electrodes are grounded and the deformation of the sample is limited. In the right frame, we display the IPMC deflection for the same voltage V_{IPMC}, but with electrostatic actuation. The magnification of the IPMC deformation due to the electrostatic pressure triggers the pull-in phenomenon, thereby causing the IPMC to touch one of the electrodes.

To examine the onset of pull-in as a function of V_{IPMC} and V_{Wall}, we systematically vary V_{IPMC} and V_{Wall} in a series of experiments. The voltage applied across the IPMC spans from 1.3 V to 1.7 V in steps of 0.1 V, while the voltage across the external electrodes varies from 0 to 4 kV in increments of 1 kV, resulting in a 5×5 grid of (V_{IPMC}, V_{Wall}). For each voltage pair, we score the number of trials in which the IPMC touches one of the external electrodes. To control for the effect of the initial eccentricity and asymmetries in the experimental setup, we test the sample under four different configurations (inverting the polarity of V_{IPMC} and the orientation of the sample). For each configuration and voltage pair, we perform ten repetitions, totaling 1000 trials. The order of the trials is randomized over the value of V_{IPMC}, the orientation of the sample, and the polarity of V_{IPMC}, to avoid potential hysteretic effects that may act as experimental confounds. The order in which the voltages V_{Wall} are applied, instead, is not randomized to mitigate the effect of residual charges.

The experimental procedure consists of the following steps. The IPMC, initially in deionized water, is completely dabbed. The tip of the sample, which will not be in contact with the copper strips on the clamps, is dipped again into water. The tip of the specimen is then slightly dabbed again to avoid deposition of water on the external electrodes. The sample is finally installed in the clamping and positioned between the external electrodes. The voltage pairs are selected from the laptop for an experimental window of five seconds, in which the trial is recorded. At the end of the trial, the IPMC is removed from the clamps and stowed in water for 1 min to avoid excessive dehydration. Every 20 trials in the series, the sample is kept in water for a resting period of five minutes to minimize the effect of drying.

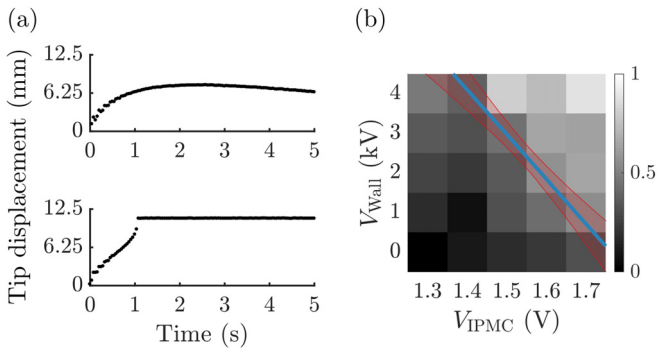

FIG. 2. (a) Time evolution of the tip displacement for the two cases shown in Fig. 1(b), that is, $V_{\text{IPMC}} = 1.4$ V, $V_{\text{Wall}} = 0$ kV (top) and $V_{\text{IPMC}} = 1.4$ V, $V_{\text{Wall}} = 4$ kV (bottom). (b) Experimental map of the ratio of the number of contacts with the external electrodes over the number of trials. The line (blue) indicates the 50% success curve of the logistic regression over the experimental data; 95% confidence band (red) is also shown.

Figure 2(a) presents the time trace of the tip displacement shown in Fig. 1(b), identified through image processing of the tests. Image analysis confirms that the experimental time window is sufficiently large to capture the entire dynamics of the actuation, although a mild back-relaxation[31] can be noted in the top panel where the IPMC starts to bend backwards under the same applied voltage V_{IPMC}. Figure 2(b) synoptically illustrates the probability of the IPMC touching one of the external electrodes for each voltage pair. In agreement with our expectations, for a given V_{Wall}, increasing the IPMC voltage causes an increase in the probability that the sample touches the wall. As an indirect measure of the onset of pull-in, we fit a logistic regression model[32] of the probability of touching one of the external electrodes, with V_{IPMC} and V_{Wall} as explanatory variables, to obtain the line with 50% probability of contact.

To shed light on our experimental findings, we put forward a structural model along with a reduced-order solution. The model accounts for the internal actuation of the IPMC, represented by a uniform bending moment M_{IPMC}, the distributed loading f_{es} due to the electrostatic pressure, and an initial eccentricity w_{in}. The initial eccentricity, although not producing any elastic force, is responsible for a non-zero net electrostatic force on the IPMC in the absence of internal actuation. We denote with $w(x) = w_{\text{el}}(x) + w_{\text{in}}(x)$ the total lateral displacement of the sample, where w_{el} is the elastic contribution and x the abscissa along the axis from 0 to the free length $L = 40$ mm. The governing equation for $w(x)$ is

$$EIw_{\text{el}}'''' = f_{\text{es}}(w), \tag{1}$$

where superimposed prime means differentiation. The boundary conditions for the problem are $w(0) = 0$, $w'(0) = 0$, $EIw_{\text{el}}''(L) + M_{\text{IPMC}} = 0$, and $EIw_{\text{el}}'''(L) = 0$. Since M_{IPMC} is constant with respect to the abscissa, it only appears in the boundary conditions of the problem. The bending stiffness EI is determined to be 2.32×10^{-6} N m^2 from vibration tests,[33] by fitting on the fundamental resonance frequency under base excitation. The bending moment due to IPMC actuation is assumed to be proportional to the voltage applied across it, that is, $M_{\text{IPMC}} = \alpha V_{\text{IPMC}}$, following standard practice in phenomenological models of IPMC actuation.[34] The electromechanical coupling coefficient α is identified as 1.49×10^{-5} N m/V from independent experimental trials, through a linear regression on tip deflection data as a function of the applied voltage. The electrostatic loading depends on the inverse of the total lateral displacement w, as follows:[35]

$$f_{\text{es}}(w) = \frac{1}{2}\varepsilon b V_{\text{Wall}}^2 \left(\frac{1}{(g_0 - w)^2} - \frac{1}{(g_0 + w)^2} \right), \tag{2}$$

where ε is the air dielectric constant ($\varepsilon = 8.854 \times 10^{-12}$ F/m) and b is the IPMC width. For convenience, we introduce nondimensional variables $\tilde{x}$ and $\tilde{w}$, such that $x = L\tilde{x}$ and $w = g_0\tilde{w}$.

To solve the nonlinear differential model in Eq. (1), the elastic contribution to the lateral displacement is approximated via two shape functions, such that $\tilde{w}_{\text{el}}(\tilde{x}) \approx \Psi_1(\tilde{x})\delta_1 + \Psi_2(\tilde{x})\delta_2$, with the normalization conditions $\Psi_1(1) = 1$ and $\Psi_2(1) = 1$. We select these shape functions based on the individual effect of V_{IPMC} and V_{Wall} on the IPMC deflection. $\Psi_1(\tilde{x})$ corresponds to the static deflection of a beam under distributed uniform load, which would correspond to the linearized solution of Eq. (1) with $V_{\text{IPMC}} = 0$ and moderate values of V_{Wall}.[35] On the other hand, $\Psi_2(\tilde{x})$ represents the static deflection of a beam under uniform bending, corresponding to the solution of Eq. (1) with $f_{\text{es}} = 0$. Using the Galerkin method,[36] we substitute the proposed approximation in Eq. (1) to obtain a nonlinear algebraic system for δ_1 and δ_2.

Figure 3(a) shows δ_1 and δ_2 as functions of V_{IPMC} and V_{Wall} from the solution of Eq. (1). The monotonic increase in both δ_1 and δ_2 as functions of V_{Wall}, for a given V_{IPMC}, constitutes the sought enhancement in IPMC actuation due to electrostatic pressure, whereby $\delta_1 + \delta_2 = \tilde{w}_{\text{el}}(1)$. Given our choice of shape functions, δ_1 is mainly associated with electrostatic actuation, while δ_2 is primarily related to the internal actuation. Although δ_2 remains dominant throughout the considered range of actuation voltages, δ_1 becomes significant near the instability region. This is independently confirmed by fitting the shape functions [Fig. 3(b)] to the deflection from the trials in Fig. 1(b). Notably, the inclusion of the second shape function increases the adjusted R^2 of the fit from 0.40 to 0.95, offering evidence for the need of utilizing two shape functions in the projection.

The pull-in instability contour separates the stable regime in which electrostatic actuation can be effectively used to enhance IPMC performance, from the unstable regime in which electrostatic actuation has the detrimental role of forcing the IPMC to touch the external electrodes. This contour is obtained from the governing non-linear system using the so-called displacement iteration pull-in extraction (DIPIE) scheme.[37] Specifically, for a chosen value of V_{IPMC} and a given iteration, we select a value of the tip displacement, $\tilde{w}(1)$, and solve the nonlinear system for V_{Wall}, δ_1, and δ_2. Treating the tip displacement as the driving parameter, rather than V_{Wall}, allows for obviating to the polydromy of the contour. The equilibrium voltage V_{Wall} is computed for different values of the normalized tip displacement, as shown in Fig. 3(c). The pull-in voltage is the maximum value of V_{Wall}, separating the stable from the unstable region.

The initial eccentricity has an important role in the pull-in instability contour, by anticipating the onset of the

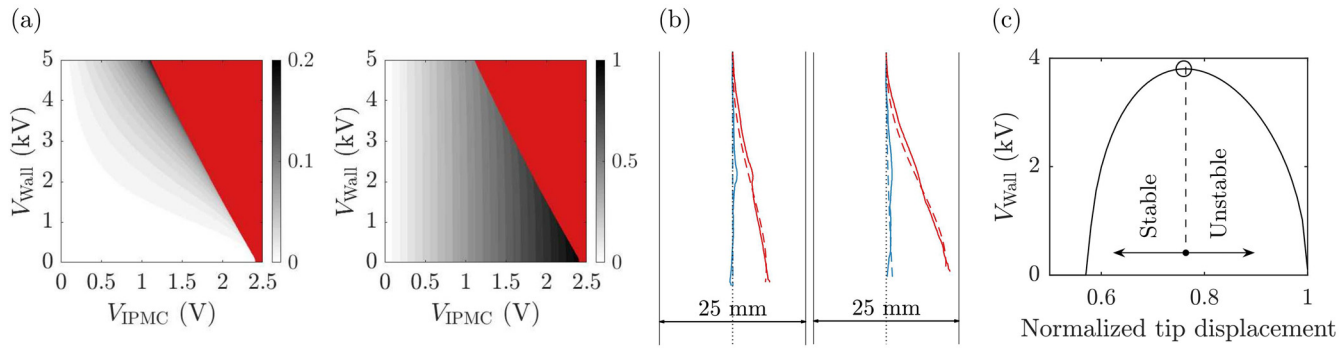

FIG. 3. (a) Theoretical prediction of δ_1 (left) and δ_2 (right) for different values of the input voltages with null initial eccentricity. The red area is the pull-in instability region. (b) Initial (blue) and final (red) deflection of the IPMC specimen for the two cases shown in Fig. 1(b). The solid lines represent the experimental data from image processing, while the dashed ones are fitted data using two shape functions introduced in the reduced-order model. (c) Illustration of the DIPIE algorithm for $V_{\text{IPMC}} = 1.4$ V. The curve represents the electrostatic equilibrium, as the nondimensional tip deflection is varied from 0 to 1.

instability. From Eq. (2), the presence of an initial prebending of the IPMC will, in fact, elicit an increase in the electrostatic loading, thereby triggering an earlier onset of the pull-in phenomenon. By hypothesizing that w_{in} corresponds to uniform bending, from image analysis, we estimate a standard deviation in the tip deflection due to the eccentricity of 0.59 mm. In Fig. 4, we present a sensitivity analysis for the pull-in instability contour, where, for completeness, we also vary the electromechanical coupling coefficient that from experimental identification was found to display a relatively large standard deviation of 3.24×10^{-6} N m/V. The sensitivity analysis is conducted by solving the nonlinear reduced order model, while drawing α and w_{in} uniformly from the identified ranges. Therein, we also display the logistic regression estimated in Fig. 2(b), which is in good agreement with theoretical prediction on the onset of pull-in instability, upon taking into consideration salient statistical variations from IPMC eccentricity and actuation.

In this letter, we have analyzed a method to enhance IPMCs' deformation via the synergistic use of electrostatic forces acting on the IPMC electrodes. Via external electrodes, we induce an electric field around the IPMC, which, in turn, creates an electrostatic pressure whose net effect acts in coordination with IPMC internal actuation. The range of operation of this approach is defined by the pull-in phenomenon, whereby the IPMC configuration will lose stability above a critical voltage and spontaneously touch one of the external electrodes. Through principled experiments and physically based modeling, we have demonstrated the viability of the approach and shed light on the nonlinear physics underpinning IPMC actuation, due to the combined effects of chemoelectrical and electrostatic forces. This study opens the door for the systematic integration of multiple IPMC physical mechanisms toward its engineered performance.

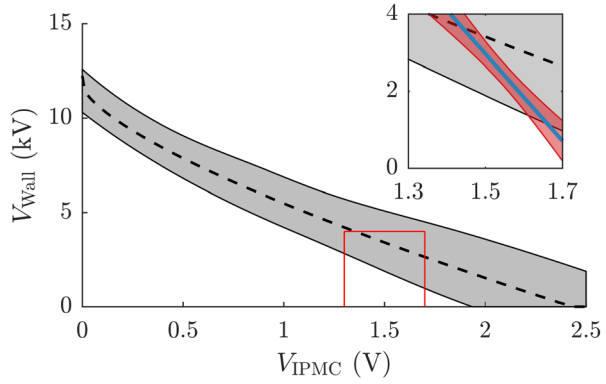

FIG. 4. Theoretical envelope of the pull-in instability curve, obtained from a sensitivity analysis on the coupling coefficient and initial prebending, within one standard deviation of experimental variation. The dashed line represents the pull-in instability curve for the mean value of α, with no eccentricity. In the inset, corresponding to the red box, we show the comparison between the theoretical envelope and the logistic regression from Fig. 2(b).

See supplementary material for image analysis, vibration tests for the identification of the bending stiffness, independent trials on the electromechanical coupling, and convergence analysis for the reduced-order model.

This research was supported by the National Science Foundation under Grant No. OISE-1545857 and by KIST flagship program under Project No. 2E28250.

[1]C. Jo, D. Pugal, I.-K. Oh, K. J. Kim, and K. Asaka, Prog. Polym. Sci. **38**, 1037 (2013).
[2]*Ionic Polymer Metal Composites (IPMCs), Smart Materials Series*, edited by M. Shahinpoor (The Royal Society of Chemistry, 2016), Vol. 1.
[3]Z. Chen, Rob. Biomimetics **4**, 24 (2017).
[4]S. Ruiz, B. Mead, V. Palmre, K. J. Kim, and W. Yim, Smart Mater. Struct. **24**, 015007 (2015).
[5]U. Deole, J. Simpson, and R. Lumia, *Ionic Polymer Metal Composites (IPMCs): Smart Multi-Functional Materials and Artificial Muscles* (The Royal Society of Chemistry, 2016), Vol. 1, pp. 386–402.
[6]T. Horiuchi, T. Mihashi, T. Fujikado, T. Oshika, and K. Asaka, Smart Mater. Struct. **26**, 045021 (2017).
[7]J. D. Carrico, T. Tyler, and K. K. Leang, Int. J. Smart Nano Mater. **8**, 144 (2017).
[8]M. Porfiri, H. Sharghi, and P. Zhang, J. Appl. Phys. **123**, 014901 (2018).
[9]P. G. de Gennes, K. Okumura, M. Shahinpoor, and K. J. Kim, EPL (Europhys. Lett.) **50**, 513 (2000).
[10]D. Schicker and T. Wallmersperger, J. Appl. Phys. **114**, 163709 (2013).
[11]S. Nemat-Nasser and C. W. Thomas, in *Electroactive Polymer (EAP) Actuators as Artificial Muscles: Reality, Potential, and Challenges*, edited by Y. Bar-Cohen (SPIE, 2004), pp. 171–230.
[12]M. Shahinpoor, Y. Bar-Cohen, J. Simpson, and J. Smith, Smart Mater. Struct. **7**, R15 (1998).
[13]B. Bhandari, G.-Y. Lee, and S.-H. Ahn, Int. J. Precis. Eng. Manuf. **13**, 141 (2012).
[14]J. Videler, *Fish Swimming, Chapman & Hall Fish and Fisheries Series* (Springer, Netherlands, 1993).
[15]Z. Chen, T. I. Um, and H. Bart-Smith, Sens. Actuators, A **168**, 131 (2011).
[16]B. J. Akle, M. D. Bennett, and D. J. Leo, Sens. Actuators, A **126**, 173 (2006).

[17]M. Farid, Z. Gang, Y. M. Zhu, A. Chatto, and R. A. Javed, *Materials Technologies, Automation Systems and Information Technologies in Industry, Applied Mechanics and Materials* (Trans Tech Publications, 2013), Vol. 389, pp. 298–303.
[18]S. J. Kim, I. T. Lee, and Y. H. Kim, Smart Mater. Struct. **16**, N6 (2007).
[19]V. Palmre, D. Pugal, K. J. Kim, K. K. Leang, K. Asaka, and A. Aabloo, Sci. Rep. **4**, 6176 (2014).
[20]S. J. Kim, I. T. Lee, H.-Y. Lee, and Y. H. Kim, Smart Mater. Struct. **15**, 1540 (2006).
[21]K. S. Lee, B. J. Jeon, and S. W. Cha, Smart Mater. Struct. **19**, 065029 (2010).
[22]J. H. Park, S. W. Lee, D. S. Song, and J. Y. Jho, ACS Appl. Mater. Interfaces **7**, 16659 (2015).
[23]J.-W. Lee, J.-H. Kim, Y. S. Chun, Y. T. Yoo, and S. M. Hong, Macromol. Res. **17**, 1032 (2009).
[24]J. A. Pelesko and D. H. Bernstein, *Modeling MEMS and NEMS* (CRC Press, 2002).
[25]K. J. Kim, V. Palmre, T. Stalbaum, T. Hwang, Q. Shen, and S. Trabia, Mar. Technol. Soc. J. **50**, 24 (2016).
[26]H. C. Nathanson, W. E. Newell, R. A. Wickstrom, and J. R. Davis, IEEE Trans. Electron Devices **14**, 117 (1967).
[27]W.-M. Zhang, H. Yan, Z.-K. Peng, and G. Meng, Sens. Actuators, A **214**, 187 (2014).
[28]W.-C. Chuang, H.-L. Lee, P.-Z. Chang, and Y.-C. Hu, Sensors **10**, 6149 (2010).
[29]R. Batra, M. Porfiri, and D. Spinello, Smart Mater. Struct. **16**, R23 (2007).
[30]K. J. Kim and M. Shahinpoor, Smart Mater. Struct. **12**, 65 (2003).
[31]K. Asaka, K. Oguro, Y. Nishimura, M. Mizuhata, and H. Takenaka, Polym. J. **27**, 436 (1995).
[32]D. A. Freedman, *Statistical Models: Theory and Practice* (Cambridge University Press, 2009).
[33]H. Harris and G. Sabnis, *Structural Modeling and Experimental Techniques*, 2nd ed. (CRC Press, 1999).
[34]Y. Cha and M. Porfiri, J. Mech. Phys. Solids **71**, 156 (2014).
[35]R. C. Batra, M. Porfiri, and D. Spinello, J. Microelectromech. Syst. **15**, 1175 (2006).
[36]T. Mura and T. Koya, *Variational Methods in Mechanics* (Oxford University Press, 1992).
[37]O. Bochobza-Degani, D. Elata, and Y. Nemirovsky, J. Microelectromech. Syst. **11**, 612 (2002).